The Structure of the Chiral Pt{531} Surface: A Combined LEED and DFT Study

S. R. Puisto,[†] G. Held,*[,†] V. Ranea,[‡] S. J. Jenkins,[†] E. E. Mola,[‡] and D. A. King[†]

Department of Chemistry, University of Cambridge, Lensfield Road, Cambridge CB2 1EW, United Kingdom, and INIFTA (CONICET, CIC) Facultad de Ciencias Exactas, Universidad Nacional de La Plata, La Plata, Argentina

Received: June 20, 2005; In Final Form: September 27, 2005

The structure of the chiral kinked Pt{531} surface has been determined by low-energy electron diffraction intensity-versus-energy (LEED-IV) analysis and density functional theory (DFT). Large contractions and expansions of the vertical interlayer distances with respect to the bulk-terminated surface geometry were found for the first six layers (LEED: $d_{12} = 0.44$ Å, $d_{23} = 0.69$ Å, $d_{34} = 0.49$ Å, $d_{45} = 0.95$ Å, $d_{56} = 0.56$ Å; DFT: $d_{12} = 0.51$ Å, $d_{23} = 0.55$ Å, $d_{34} = 0.74$ Å, $d_{45} = 0.78$ Å, $d_{56} = 0.63$ Å; $d_{bulk} = 0.66$ Å). Energy-dependent cancellations of LEED spots over unusually large energy ranges, up to 100 eV, can be explained by surface roughness and reproduced by applying a model involving 0.25 ML of vacancies and adatoms in the scattering calculations. The agreement between the results from LEED and DFT is not as good as in other cases, which could be due to this roughness of the real surface.

1. Introduction

Intrinsically chiral surfaces, i.e., surfaces with no mirror or glide symmetry, are seen as potential templates for heterogeneous enantioselective catalysis and present, therefore, an enticing technological opportunity for modern surface science.[1−6] It has been shown in both electrochemical[3,4,7] and ultrahigh vacuum (UHV) experiments[8] that enantioselective reactions may occur on such surfaces. Whenever surfaces of fcc crystals are characterized by three inequivalent nonzero Miller indices[1,3] they are chiral. Their consequent structural complexity also partially bridges the materials gap between flat crystal facets and more open structures as they can be found on real catalyst nanoparticles with a high density of low-coordinated kink atoms, which often exhibit higher reactivity than terrace atoms. Both phenomena, enentioselectivity and increased catalytic activity, are intimately connectcted with the surface geometry. A detailed microscopic understanding can, therefore, only be achieved if the surface structure is known precisely.

In common with all intrinsically chiral fcc single-crystal surfaces, Pt{531}, which is the subject of the current study, displays microfacets of {111}, {100}, and {110} nature. An extension of the Cahn−Ingold−Prelog rules proposed by Ahmadi et al.[3] provides a convenient nomenclature for the present situation: if the sequence of microfacets meeting at each kink reads {111}-{100}-{110} in a clockwise direction when viewed from above then the surface will be denoted "R", otherwise it will be denoted "S". A recently proposed alternative convention, based instead upon the spatial relationship between the surface normal and the high-symmetry ⟨111⟩, ⟨100⟩, and ⟨110⟩ directions, leads to a designation of "D" for fcc-"R" and "L" for fcc-"S" surfaces.[9]

In general, if one type of microfacet is considered to correspond to a set of surface terraces, then the other two microfacet types will be seen to form regularly kinked steps between those terraces. For this reason, fcc chiral surfaces are often described as "kinked". Where all three microfacets meet, we find the "kink" itself, a 6-fold coordinated atom, which is generally assumed to be a particularly active site for catalysis. These atoms have no nearest neighbors in the top-most atomic layer, which is the reason adatom-vacancy pairs can be formed at very little cost in energy and potentially cause significant roughness of these surfaces possibly affecting their enantioselectivity.[2,9−12]

Despite the potential importance of these surfaces, information regarding their detailed atomic structure is almost entirely absent from the literature. The lack of symmetry in chiral surfaces certainly poses a major problem in terms of both theoretical and experimental analysis. Less obviously, the fact that layer spacings perpendicular to high-Miller-index surfaces tend to be small (0.66 Å for Pt{531}) causes problems for both surface crystallography by low-energy electron diffraction (LEED) and first-principles density functional theory (DFT), which will be discussed in detail later. Despite the large atomic corrugation, to date there are also no unambiguous data from scanning tunneling microscopy (STM) on kinked surfaces.[13−15] Especially the magnitudes and directions of relaxations near the kink atoms are unclear, which have direct influence on the effective coordination and, hence, upon the reactivity of the surface. There are, however, an increasing number of examples in the more recent literature where the above-mentioned problems with LEED have been mastered[16−23] and detailed crystallographic information was extracted for a number of stepped surfaces. Also the rapid increase in computational power makes complex surface geometries more accessible to ab initio model calculations. The {531} surface of Pt (see Figure 1) has been chosen for the present study because of its particularly small surface unit cell, which reduces the computer time consumed for LEED and DFT model calculations as compared to other chiral surfaces. In addition to the kink atom in the upper-most atomic layer, Pt{531} has under-coordinated atoms with 8, 10, and 11 nearest neighbors in the second, third, and fourth layer, respectively. This surface is the simplest kinked chiral surface;

* Address correspondence to this author. address. E-mail: gh10009@cam.ac.uk.
[†] University of Cambridge.
[‡] Universidad Nacional de La Plata.

10.1021/jp053321b CCC: $30.25
Published on Web 11/08/2005

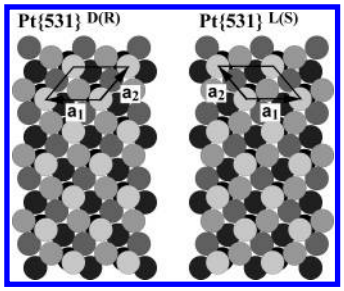

Figure 1. Schematic drawing of the ideal Pt{531}$^{D(R)}$ and Pt{531}$^{L(S)}$ surfaces The brightness of the circles corresponds to the height of the atoms (upper-most atoms are lightest). Note that, against the convention, the lattice vectors of the D(R) surface are drawn as a left-handed system to make them compatible with the beam indices in Figure 3.

none of the "facets" {111}, {100}, {110} has actually a complete surface unit cell exposed. The present article provides the first detailed structure determination of an intrinsically chiral surface. It demonstrates some of the problems imposed by the complexity of the surface and shows how LEED and DFT may fruitfully be combined to obtain high-quality data on the atomic and electronic structure of these intriguing surfaces.

2. Experimental Details and Calculations

2.1. Experimental Procedures. The experiments were carried out in an UHV system with a base pressure of 5×10^{-11} mbar, described elsewhere.[24] The Pt single crystal was oriented by using Laue diffraction and cut by spark erosion parallel to the {531} crystallographic plane within 0.5°. The crystal face used for the experiments was Pt{531}$^{L(S)}$, as determined by LEED (see below) and later confirmed by Laue diffraction.

The surface was cleaned by using standard procedures including Ar ion sputtering (500 eV/ 7 μA for 30 min), annealing in oxygen (5×10^{-7} mbar/1100 K for 15 min), flashing to 1150 K (1 min), and cycles of CO adsorption/desorption (300 to 600 K). Auger electron spectroscopy and CO temperature programmed desorption (TPD) were used to check the surface cleanliness. CO TPD proved to be particularly sensitive to low levels of carbon and oxygen contamination.

After this treatment the spots of the $p(1 \times 1)$ diffraction pattern are observed with some additional diffuse features at certain energies, indicating a relatively high degree of surface roughness. Examples of the observed LEED patterns are shown in Figure 2. The IV curves for each spot show extended regions, up to 100 eV wide, of zero intensity, where the spot intensity cannot be distinguished from the background (below 2% of maximum intensity).

LEED-IV data were recorded over the energy range 30−300 eV at a sample temperature of 200 K with a video-rate CCD camera. The electron energy was ramped in steps of 1 eV and 4 images were recorded and averaged for each energy step, using the AIDA-PC program (SPECS). Since there is no risk of damaging a clean metal surface by a low-energy electron beam in the μA range, a relatively high beam current of around 4 μA was used. This has the advantage of a high signal-to-noise ratio and short data acquisition times (less than 10 min), avoiding surface contamination with residual gases. The spot intensities were extracted off-line from the recorded images with a homemade program (MKIV[25]). The program records the intensities of all visible spots at once and determines the reciprocal lattice from their positions. Therefore, the traces of spots with zero intensity are not lost even for extended "dark" periods. Finally, the IV curves were processed with use of Fourier transform smoothing to eliminate the high-frequency noise without affecting the significant peak structure. The cutoff frequency corresponds to features 4 eV wide.

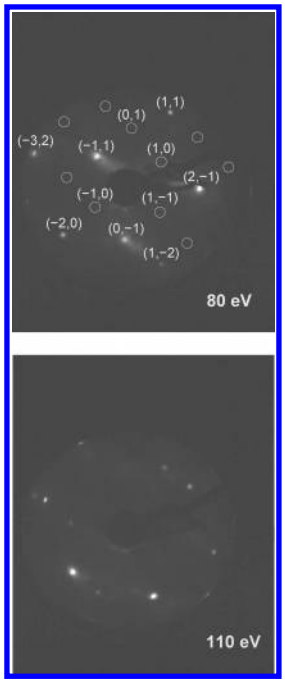

Figure 2. Experimental LEED patterns observed for electron energies of 80 (top) and 110 eV (bottom). The indices of all visible spots and the zero-intensity spots of the inner circle are indicated in the top panel. The positions of spots with zero intensity at this energy are indicated by circles.

Because the Pt{531} surface has no symmetry, normal incidence cannot be achieved in the usual way by comparing symmetry-equivalent beams. Instead the sample was adjusted by eye close to normal incidence and the polar and azimuthal angles of incidence were incorporated as additional search parameters in the structural analysis with starting values estimated from the spot positions in the recorded LEED images.

2.2. LEED-IV Analysis. The model calculations for the LEED structure determination were performed with our "CLEED" program package,[26] which is an implementation of fully dynamical scattering theory based on algorithms described by Pendry[27] and Van Hove and Tong.[28] Because of the small interlayer distance of 0.66 Å, layer doubling could not be employed and the reflection matrix for the entire surface had to be calculated by using the combined space or "giant matrix inversion" method. The surface was modeled by using a stack of 16 layers (≈10 Å) after test calculations had shown that increasing the stack thickness beyond this number did not lead to significant changes in the IV curves. Test calculations with similar stack thickness were performed for other stepped and kinked surfaces, for which experimental data and surface geometries are published,[20,21] to ensure the validity of this approach.

LEED intensities were calculated for electron energies between 30 and 230 eV in steps of 4 eV. The constant damping potential V_{0i} was set to 5.8 eV, which is equivalent to the inelastic mean free path of around 5 Å in the relevant energy range.[29] The rms displacement used for the bulk Pt atoms with full coordination, 0.035 Å, was optimized with experimental data from Pt{111}; it is significantly lower than the value of 0.07 Å, calculated from the Debye temperature of Pt, 230 K,[30] and the sample temperature of 200 K. For the four upper-most layers, where the atoms have lower coordination, the rms displacement was set to 0.050 Å. The scattering phase shifts

for the platinum atoms were calculated with the program package provided by Barbieri and Van Hove.[31] Phase shifts were used up to a maximum angular momentum quantum number l_{max} equal to 8.

For the structure optimization and the determination of the angles of incidence the downhill simplex method[32,33] was used. The convergence criterion was that the *R* factor values did not change within 1×10^{-4}. In most cases Pendry's R_P and *RR* factors[34] were used to compare experimental and theoretical IV curves in the geometry optimization and for estimating the error margin of each geometry parameter, respectively. Data from 30 spots were used in the analysis. Since the surface has no symmetry, the IV curves of all spots are different from each other, which leads to a large cumulative energy overlap of inequivalent spots. However, since logarithmic derivatives are used in the calculation of Pendry's R_P factor,[34] the zero-intensity parts of the IV curves could not be used. Fluctuations of the experimental intensities in these energy regions would lead to unreliable values of R_P. Therefore, the usable energy range, ΔE, was reduced to 1920 eV, which results in a *RR* factor ($\sqrt{8V_{0i}/\Delta E}$) of 13%.[34] More details about the error estimate can be found in ref 35.

To make use of the full experimental data set, in some cases a different *R* factor, R_2, was used, defined as follows:

$$R_2(I_e,I_t) = \frac{\int\left(I_t - \sqrt{\frac{\int I_t^2}{\int I_e^2}}\cdot I_e\right)^2 dE}{\int (I_t - \langle I_t\rangle)^2\, dE}, \qquad (1)$$

$I_{e,t}$ are the intensities of the experimental and the theoretical IV curves, respectively. This is somewhat different from the standard definition[36] or Adams' definition[37] since the integral in the denominator is over the square of the difference between I_t and the average intensity, $\langle I_t\rangle$, rather than just over I_t^2. This modification ensures, however, that uncorrelated IV curves lead to an R_2 value around 1, which makes the values better comparable with those of R_P.

2.3. DFT Calculations. The DFT calculations were performed by using the CASTEP computer code[38,39] in a supercell of length equivalent to 30 {531} layers of Pt in the surface-normal direction, and the surface itself was represented by a slab of 18 such layers. The experimental lattice constant (a = 3.92 Å) was used in defining the lateral periodicity of the model geometry. The unusually large number of layers is necessary because of the small interlayer spacing (0.66 Å for bulk). A (1×1) surface unit cell was assumed; this lack of reconstruction was borne out by the LEED experiments. Electronic wave functions were expanded in a basis set of plane waves up to a 340 eV kinetic energy cutoff, and the Brillouin zone was sampled at a $3 \times 3 \times 1$ mesh of Monkhorst−Pack special *k*-points.[40] Exchange-correlation effects were included through the Perdew−Wang form of the generalized gradient approximation,[41] and the electron−ion interaction was dealt with through the use of ultrasoft pseudopotentials.[42] Six atomic layers on one side of the slab were allowed to relax according to the calculated forces, while the remaining layers were held fixed at their bulk positions.

3. LEED Results

The chiral orientation of the surface was not known a priori and could not be determined from the positions of the LEED spots. Therefore, four different crystal orientations had to be tested for each class of trial geometries. These are indicated in Figure 3, they include the mirror operation, which converts the D (R) surface into L (S), and a rotation by 180° which leaves the positions of the LEED spots unchanged, however, not their intensities. All calculations were performed for the $\{531\}^{L(S)}$ surface shown in Figure 1 (right panel). Instead of applying rotation and mirror operations to the actual trial geometries, the indices of the experimental IV curves to be compared within the R_P factor analysis were swapped accordingly.

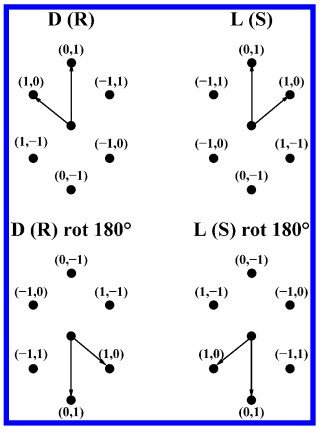

Figure 3. Schematic view of the Pt{531} LEED pattern and the four possibilities to index the beams: D(R) and L(S) chiralities, which are related by a mirror operation, and the rotation by 180°.

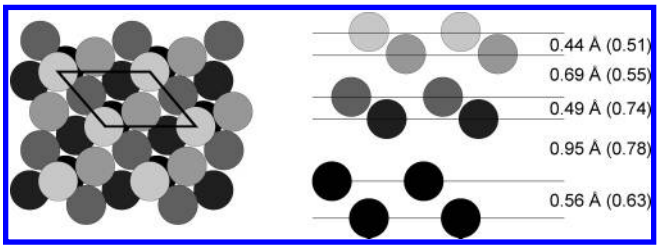

Figure 4. Schematic top view (left) and side view (right) of the best-fit LEED structure for Pt{531} with alternating contractions and expansions of the first five layers. The numerical values indicated for the vertical distances are those found by the R_P analysis; the values in brackets are those from the DFT calculations (cf. Table 2).

The coordinates of the atoms in the top-most 6 layers were optimized in two steps, in the first only the vertical and in the second all three atomic coordinates were varied. In both steps R_P was used and only the nonzero parts of the experimental IV curves were compared with the theoretical curves. In total, 18 geometric parameters plus 2 angles of incidence were optimized with a cumulative energy range of about 100 eV per parameter. The fact that a (1×1) periodicity is observed experimentally does not allow much freedom for surface reconstructions. The number of trial structures is therefore rather limited. Several start geometries with lateral bulk positions and different interlayer spacings were tested, which all converged to the same R_P factor minimum of 0.292 for interlayer distances of 0.44 (d_{12}), 0.70 (d_{23}), 0.50 (d_{34}), 0.94 (d_{45}), and 0.56 Å (d_{56}) and lateral displacements from the bulk positions between 0.04 and 0.11 Å (see Figure 4). The vertical distances between the layers correspond to alternating contractions and expansions with respect to the bulk interlayer distance of 0.66 Å.

Another type of trial geometries was inspired by the results of a recent XPS study, which found that there is a very stable oxygen species left behind on Pt{531} after normal oxygen treatment.[43] This was assigned to oxide clusters on the surface rather than to a subsurface oxygen species. Despite this assignment, structures involving subsurface oxygen were considered in the LEED analysis. In particular, an oxygen atom

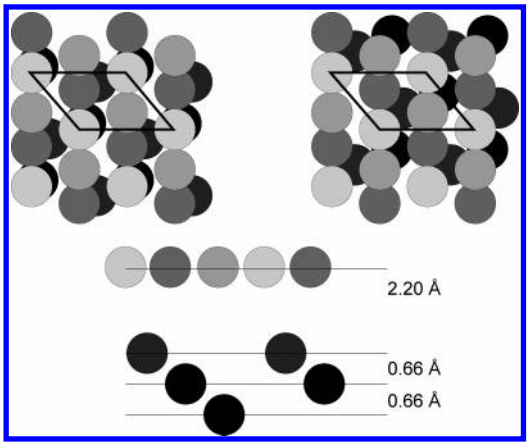

Figure 5. Structures with three atoms in a quasihexagonal arrangement in the top-most layer. Top views of the two possibilities, which differ in their registry with respect the platinum atom in the next layer, are shown in the upper panel. A schematic side view is shown in the bottom panel.

TABLE 1: The Pt{531} Structural Models Studied by LEED-IV with Associated R_P Factors[a]

structure	R_P ($RR = 13\%$)
contractions and expansions of the first five layers (− + − +) (Figure 4)	0.29
DFT structure with double contraction, double expansion (− − + +) (Figure 4)	0.47
bulk-terminated structure with interlayer spacings of 0.663 Å	0.68
subsurface oxygen between the 4th and 5th platinum layer	0.34
3 atoms in the top-most layer, model 1 (Figure 5, left)	0.65
3 atoms in the top-most layer, model 2 (Figure 5, right)	0.65

[a] See text for details.

incorporated between the fourth and fifth Pt layer might explain the surprisingly large distance of over 0.9 Å between these two layers, which corresponds to an expansion of about 40% with respect to the bulk interlayer spacing. The lowest R_P factor found for this type of structures is 0.34, just outside the error bars of the best fit geometry. Therefore, this structure can also be disregarded. The Pt positions for this geometry are almost unchanged with respect to the oxygen-free best fit structure, which illustrates that the LEED intensities are rather insensitive to extra oxygen atoms buried in the surface, due to the large depth and their small scattering strength compared to Pt.

The only trial structure that is fundamentally different from the bulk-terminated geometry is shown in Figure 5. It is similar to the hexagonal reconstruction of the clean Pt{100} surface[44,45] in that the three top-most Pt atoms are essentially coplanar forming one quasihexagonal {111}-like layer. This layer can be arranged with respect to the atoms underneath in two different ways, as shown in Figure 5. The optimization of both structures converged at almost identical R_P values around 0.65, which are clearly outside the error margins of the best fit structure above.

Table 1 summarizes the lowest R_P factors found for all tested trial structures and, for comparison, the R_P factors for the bulk-terminated surface and the geometry found by DFT (see below). Clearly, the surface geometry with alternating contracted and expanded vertical distances between the five upper-most layers (see Figure 4) is favored above all others.

As mentioned before, the extended energy regions of zero intensities were not included in this LEED-IV analysis so far, mainly for technical reasons related to Pendry's R_P factor, although the cancellation of spot intensities carries important information. When the calculated IV curves for the best fit structure are visually compared with the experimental IV curves over the complete energy range, intense maxima in the theoretical curves are found also in energy regions where the experimentally observed IV curves are zero. None of the tested geometry models led to extended zero-intensity regions of the size observed experimentally. Also variations of the nongeometrical parameters (thermal displacements, inelastic mean free path, stack thickness) did not improve the agreement in these parts of the IV curves. The only way of reproducing the zero-intensity parts in the theoretical IV curves was by assuming a relatively high degree of surface roughness.[12] A simple model with equal coverages, Θ_{ad}, of adatoms and vacancies at the positions of atoms in the next layer up or down with respect to the ideal surface layer leads to an energy-dependent envelope function, which is different for each spot with index $\vec{G}$:

$$F_{\vec{G}}(E,\Theta_{ad}) = \left[1 - 4\Theta_{ad}\sin^2\left(\frac{1}{2}u_{\vec{G}}(E)\right)\right]^2 \qquad (2)$$

with

$$u_{\vec{G}}(E) = \vec{G}\cdot\vec{d}_{10,||} + \left[\left(\frac{2mE}{\hbar^2} - (\vec{k}_{in,||}(E) + \vec{G})^2\right)^{1/2}\cdot\vec{e}_{\perp} - \vec{k}_{in,\perp}(E)\right]\cdot\vec{d}_{10,\perp} \qquad (3)$$

$\vec{d}_{10}$ is the vector pointing from a Pt atom to another atom in the next layer up, $\vec{e}_{\perp}$ is a vector of unit length perpendicular to the surface; further details of the derivation can be found in a separate publication.[12] $F_{\vec{G}}(E,\Theta_{ad})$ needs to be multiplied with the IV curve for the flat surface $I_{\vec{G}}(E,\Theta_{ad} = 0)$ to calculate the curve for the rough surface.

$$I_{\vec{G}}(E,\Theta_{ad}) = I_{\vec{G}}(E,\Theta_{ad}=0)\cdot F_{\vec{G}}(E,\Theta_{ad}) \qquad (4)$$

A closer investigation of eq 2 reveals that only values of Θ_{ad} around 0.25 lead to an extinction of spot intensities over extended energy ranges.[12] This value, $\Theta_{ad} = 0.25$, was therefore used in a new search, where the theoretical IV curves were calculated according to eq 4. Now all experimental data were included in the R factor calculation, which led to a cumulative energy range of 3638 eV. To avoid problems due to the definition of Pendry's R_P factor in the zero-intensity regions, we used R_2 (see eq 1 above) instead for this structure optimization.

Starting from the best-fit geometry found before (with R_P) the new search converged to a very similar geometry with most coordinates within the error margins of the previous geometry. The envelope function of eq 4 leads to good agreement in the zero-intensity regions for all IV curves, as can be seen from Figure 6, whereas in the nonzero parts the IV curves remain essentially unchanged. The lowest R_2 value is 0.108 when the calculated IV curves are modified with the envelope function. If the envelope function is not included, the search leads to a lowest R_2 value of 0.483. The same structure optimization was also performed with R_P and the envelope function but only the nonzero parts of the experimental IV curves. This led to a lower R_P minimum of 0.263 with essentially no change in the best fit geometry as compared to the previous search without the envelope function. The complete sets of coordinates of the two best-fit geometries, found with R_P and R_2, are listed in Table 2; a selection of experimental and calculated IV curves is shown

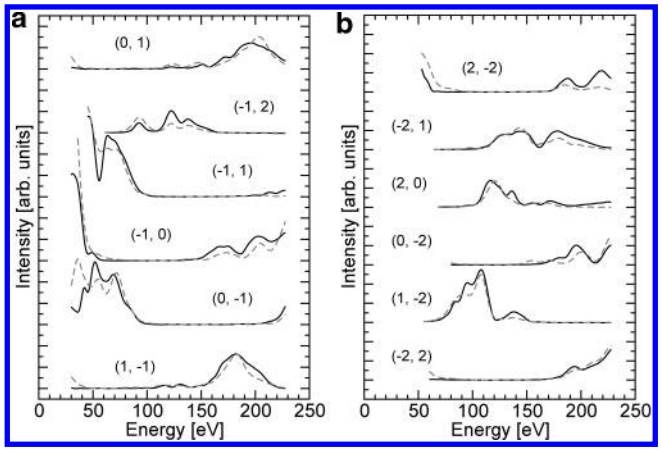

Figure 6. Selection of experimental (solid) and theoretical IV curves (dashed) of selected beams for the best fit geometry found with R_P.

in Figure 6. The Table shows that all lateral deviations from the bulk positions are within the error bars of the analysis.

4. DFT Results

DFT calculations were performed with a starting structure in which interlayer spacings were fixed at the values determined by LEED, but this changed substantially as atoms were allowed to move in response to the calculated forces. The final relaxed structure obtained from DFT features a marked pairing of signs for the changes in interlayer spacing, following the order −22%, −17%, +11%, and +18% in the first four spacings, before reverting to a simple alternation of −5 and +5% in the following two. In common with the LEED structure, therefore, the fourth interlayer spacing (i.e., between layers four and five) is the largest, but the absolute value of 0.78 Å is considerably less than that obtained by LEED. The overall pattern of relaxation also contradicts the simple alternation found in LEED. In contrast to the substantial vertical relaxations, however, DFT agrees with LEED in determining rather small lateral relaxations.

Following the same logic as was applied for the LEED analysis, we also tried placing O atoms between layers four and five, to determine whether these would indeed yield a larger spacing more in line with the experimental value. In fact, the results *did* show a substantial increase in d_{45}, but by rather too large an amount (the spacing became between 1.05 and 1.29 Å, depending upon the exact lateral position chosen for the O atom). In addition, d_{34} and d_{56} also became much larger than was found in LEED, while d_{23} became unreasonably small (less than 0.20 Å). Overall, the disagreement between these subsurface O structures and the LEED structure was far worse than when comparing structure without subsurface O. We do not, therefore, believe that subsurface O can account for the discrepancy between LEED and DFT in this case.

5. Discussion

The most striking feature of the LEED analysis is certainly that a satisfactory agreement between experiment and calculated IV curves could only be achieved by assuming a significant amount of surface roughening. Only half the surface atoms are in the ideal surface plane whereas the other half are either in the atomic layer above or below. Therefore, the result of the LEED analysis is the average geometry of the three layers involved, adatoms, vacancies, and ideal surface plane, for which we can expect the same relaxations only when the atoms are grouped into islands. This may explain some of the differences between the LEED analysis and the optimum structure from DFT, which has been found by assuming an ideally flat surface.

Since there is long-range correlation between the atoms on all three levels through the underlying bulk lattice, the LEED spots remain sharp, as seen in Figure 2, with a relatively low background level. The experimentally observed absence of sharp features in addition to the (1 × 1) LEED pattern indicates that there is no long-range superstructure in the distribution of the adatoms or vacancies, which are part of the model used to derive the envelope function in eq 2 The formation of (1 × 1) islands, however, caused by a small attractive interaction between terminating atoms at the same level cannot be excluded. It appears even likely because only then is it justified to assume that the majority of scattering factors for atoms at different levels are similar, which is another basic assumption made in the derivation of eq 2.[12] In particular, isolated vacancies should have very different scattering factors and should lead to increased background intensity, which is not observed experimentally. They are therefore unlikely to exist in large numbers. The average diameters of such islands must be well below the coherence length of the LEED experiment, which is a few hundred angstroms,[27] otherwise interference between them would not lead to the cancellation of spots. Therefore, the surface must be considered rough on the atomic scale.

For comparable surfaces with similar kinked structures, like the {210} surfaces of Al,[17] Pt,[18] Pd,[20] or Cu,[23] such extended energy ranges of zero intensity have not been reported. The most likely explanation for this difference is that their degree of roughening is less than that required for the cancellation of spot intensities. Note that for $\Theta_{ad} = 0.25$ only 50% of the surface atoms reside in the layer that would terminate the flat surface. Extended zero-intensity ranges in IV curves have been observed for Cu{320},[22] which has three lattice constants wide {110}-like terraces. The cancellation of intensities on this surface can, therefore, be explained by the convolution of diffraction patterns from the terraces and the step superstructure and is well reproduced in the model calculations for the relaxed flat surface.

The atomic structure of Pt{531} is characterized by large vertical relaxations of the individual atoms, which lead to contractions and expansions of the vertical interlayer distances of up to around 40% (LEED) with respect to the bulk value of 0.66 Å. The two LEED results, found by using different R factors and different subsets of the IV curves, agree very well, for most coordinates better than expected from the error bars of the analysis. The magnitude of relaxations in the LEED results is, however, significantly greater than those found by DFT. For d_{23} and d_{34} DFT and LEED also disagree in the signs of the relaxations. Both agree, however, that the largest contraction is in d_{12} and the largest expansion is between the fourth and fifth Pt layer.

It is difficult to decide whether one should put more weight on the LEED or DFT results. On one hand, the LEED results must be expected to be somewhat inaccurate, in particular with respect to the relaxation of the upper-most layers, due to the averaging over adatom, vacancy, and the ideal surface layer, mentioned above. On the other hand, there is very little experience with DFT studies of complex metal surfaces such as Pt{531}. Disagreements in sign and magnitude of surface reconstructions between DFT and experimental studies have been encountered even for close-packed surfaces.[46,47] Several explanations have been discussed including contaminations in the experiment or anharmonic vibrations of the outer metal atoms, which are not accounted for in DFT. Due to the short data acquistion time, contamination can be excluded in our

TABLE 2: Atomic Coordinates for the Pt{531} Surface As Determined by LEED and DFT[a]

		LEED structure ($R_p = 0.260$, $R_2 = 0.108$)					bulk-terminated			DFT structure				
atom		x	y	z	$d_{n,n+1}$	Δd	x	y	z	x	y	z	$d_{n,n+1}$	Δd
Pt_1	R_P	0.00 ± 0.13	0.00 ± 0.12	0.00 ± 0.05	0.44	−0.22 (−33%)	0.00	0.00	0.00	0.00	0.00	0.00	0.51	−0.15 (−22%)
	R_2	−0.00	0.04	0.00	0.46	−0.21 (−31%)								
Pt_2	R_P	2.54 ± 0.15	1.15 ± 0.10	-0.44 ± 0.05	0.69	+0.03 (+4%)	2.48	1.05	−0.66	2.43	1.05	−0.51	0.55	−0.11 (−17%)
	R_2	2.70	1.11	−0.46	0.61	−0.06 (−7%)								
Pt_3	R_P	-1.32 ± 0.15	2.07 ± 0.12	-1.13 ± 0.06	0.49	−0.17 (−25%)	−1.24	2.10	−1.33	−1.24	2.09	−1.07	0.74	+0.07 (+11%)
	R_2	−1.21	1.95	−1.07	0.56	−0.10 (−15%)								
Pt_4	R_P	1.23 ± 0.15	3.27 ± 0.15	-1.62 ± 0.05	0.95	+0.29 (+43%)	1.24	3.15	−1.99	1.18	3.14	−1.80	0.78	+0.12 (+18%)
	R_2	1.28	3.18	−1.63	0.93	+0.27 (+41%)								
Pt_5	R_P	0.55 ± 0.11	0.51 ± 0.10	-2.58 ± 0.06	0.56	−0.10 (−15%)	0.62	0.52	−2.65	0.58	0.54	−2.58	0.63	−0.04 (−5%)
	R_2	0.54	0.52	−2.56	0.61	−0.06 (−8%)								
Pt_6	R_P	3.13 ± 0.12	1.70 ± 0.12	-3.14 ± 0.07	0.66	−0.01 (−1%)	3.10	1.57	−3.32	3.09	1.57	−3.21	0.69	+0.03 (+5%)
	R_2	3.26	1.56	−3.16	0.62	−0.05 (−8%)								
Pt_7	R_P	−0.66	2.64	−3.79	0.66	−0.62	2.62	−3.98	−0.64	2.63	−3.90	0.66		
(bulk)	R_2	−0.62	2.62	−3.78	0.66									

[a] R_2 and R_P refer to the best fit geometries found by using the R_2 factor together with the full set of experimental data and R_P with only the non-zero parts of the experimental IV curves, respectively. See text for further details. For comparison, also the coordinates of the bulk-terminated surface are listed. All coordinates are given in Å and adjusted such that the top-most atom is at the origin of the coordinate system.

experiments, but, clearly, thermal vibrations will play an even more important role for open surfaces, such as Pt{531}, than for close-packed structures. One perennial difficulty faced when comparing LEED and DFT structures is that there is no universally agreed method for estimating errors in the latter case. One could imagine utilizing the calculated Hessian matrix (i.e., second derivative of energy with respect to atomic coordinates) to quantify the errors involved in the structure relaxation procedure, but without an unequivocal way to understand the errors in the potential energy surface (associated with the approximation of the exchange-correlation functional and the use of pseudopotentials) this can only partially account for the actual uncertainty in the result. Nevertheless, one might imagine that *reasonable* error bars for DFT structures obtained by different codes and with different versions of the GGA functional or pseudopotentials would probably be in the region of ±0.02 Å or thereabouts. In this context, and taking into account the errors of ±0.05 Å or more in the LEED vertical positions, the discrepancies in several of the interlayer spacings do not look quite so bad as they might at first appear. Only for the d_{34} and d_{45} spacings do we find a really significant disagreement (around 40% from LEED and 18% from DFT). It is also worth asking, at this stage, to what extent we should base our judgment upon the interlayer spacings or on the absolute atomic coordinates. If we align the upper-most atom in the LEED and DFT structures, as is done in Table 2 and schematically in Figure 7, we find that the discrepancy in the absolute positions of most atoms is actually pretty small—within the overlap of the error bars in most cases. Taking this view, it is clear that the major disagreement between experiment and theory is to be found in the absolute vertical position of the fourth-layer atoms, leading directly to the differences in d_{34} and d_{45} noted above. This is the lowest layer of atoms with coordination less than in the bulk. The origin of the problem in this layer remains a mystery, however.

Due to the large expansion of the distance between the fourth and the fifth layer the stack of under-coordinated atoms (layers 1−4) may appear somewhat detached from the fully coordinated atoms in the fifth layer and below. A statistical analysis of the Pt−Pt nearest neighbor distances in the LEED result, however, shows that the average bond lengths are the same, around the bulk value 2.77 ± 0.02 Å, except for the top-most layer, which has an average Pt−Pt bond length of 2.66 Å. This indicates that the average charge density is likely to be significantly different from the bulk value only in the outer-most region of the surface, near the 6-fold coordinated kink atoms, despite the openness of the surface, which leaves exposed atoms down to the fourth layer. Although the 30%/18% inward-relaxation of the kink atom makes the surface geometrically less corrugated than the bulk-terminated surface would be, this atom is still electronically distinct from the others and adsorption sites near this atom are likely to be more reactive than others.

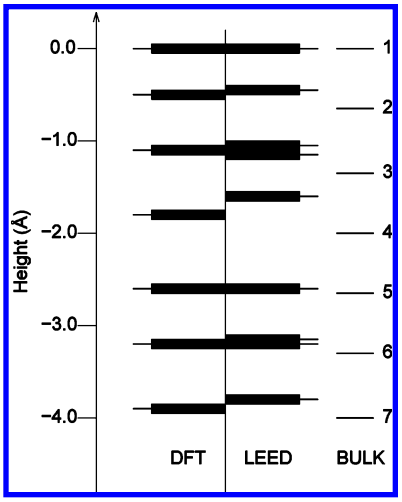

Figure 7. Comparison of the vertical atom positions in the Pt{531} surface geometries determined by LEED and DFT and in the bulk-terminated surface. Thin lines indicate the vertical positions, thick lines the error bars.

6. Conclusion

The structure of the chiral kinked Pt{531} surface at 200 K has been determined by low-energy electron diffraction intensity versus energy (LEED-IV) analysis and (at 0 K) density functional theory (DFT). Large contractions and expansions of the vertical interlayer distances, up to 43%, with respect to the bulk-terminated surface geometry were found for the first six layers. The coordination of the surface atoms, in particular the 6-fold coordinated "kink atoms", is, however, not affected by these relaxations. Pt{531} is, therefore, expected to be more reactive than flat Pt surfaces.

Energy-dependent cancellations of LEED spots over unusually large energy ranges, up to 100 eV, can be explained by surface roughness and reproduced when a model involving 0.25 ML of vacancies and adatoms is applied in the LEED scattering calculations.

Acknowledgment. The authors acknowledge the support for this study by the EPSRC through grant GR/S85528/01. S.R.P. thanks the Alfred Kordelin, Magnus Ehrnrooth, and Väisälä foundations (Finland) and Downing College, Cambridge, for financial support. S.J.J. thanks The Royal Society for a University Research Fellowship.

References and Notes

(1) McFadden, C. F.; Cremer, P. S.; Gellman, A. J. *Langmuir* **1996**, *12*, 2483.
(2) Sholl, D. S. *Langmuir* **1998**, *14*, 862.
(3) Ahmadi, A.; Attard, G. A.; Feliu, J.; Rodes, A. *Langmuir* **1999**, *15*, 2420.
(4) Attard, G. A. *J. Phys. Chem. B* **2001**, *105*, 3158.
(5) Gellman, A. J.; Horvath, J. D.; Buelow, M. T. *J. Mol. Catal. A* **2001**, *167*, 3.
(6) Downs, R. T.; Hazen, R. M. *J. Mol. Catal. A* **2004**, *216*, 273.
(7) Attard, G. A.; Ahmadi, A.; Feliu, J.; Rodes, A.; Herrero, E.; Blaise, S.; Jerkiewicz, G. *J. Phys. Chem. B* **1999**, *103*, 1381.
(8) Horvath, J. D.; Gellman, A. J. *J. Am. Chem. Soc.* **2001**, *123*, 7953.
(9) Pratt, S.; Jenkins, S. J.; King, D. A. *Surf. Sci. Lett.* **2005**, *585*, L159.
(10) Asthagiri, A.; Feibelman, P. J.; Sholl, D. S. *Top. Catal.* **2002**, *18*, 193.
(11) Power, T. D.; Asthagiri, A.; Sholl, D. S. *Langmuir* **2002**, *18*, 3737.
(12) Puisto, S. R.; Held, G.; King, D. A. *Phys. Rev. Lett.* **2005**, *95*, 036102.
(13) Sander, M.; Imbihl, R.; Schuster, R.; Barth, J. V.; Ertl, G. *Surf. Sci.* **1992**, *271*, 159.
(14) Zhao, X.; Perry, S. S. *J. Mol. Catal. A* **2004**, *216*, 257.
(15) Driver, S. M.; King, M. A. W.; King, D. A. Manuscript in preparation.
(16) Adams, D. L.; Sørensssen, C. S. *Surf. Sci.* **1986**, *166*, 495.
(17) Adams, D. L.; Jensen, V.; Sun, X. F.; Vollesen, J. H. *Phys. Rev. B* **1988**, *88*, 7913.
(18) Zhang, X. G.; Van Hove, M. A.; Somorjai, G. A.; Rous, P. J.; Tobin, D.; Gonis, A.; MacLaren, J. M.; Heinz, K.; Michl, M.; Lindner, H.; Müller, K.; Ehsasi, M.; Block, J. H. *Phys. Rev. Lett.* **1991**, *67*, 1298.
(19) Seyller, T.; Diehl, R. D.; Jona, F. *J. Vac. Sci. Technol. A* **1999**, *17*, 1635.
(20) Kolthoff, D.; Pfnür, H.; Fedorus, A. G.; Koval, V.; Naumovets, A. G. *Surf. Sci.* **1999**, *439*, 224.
(21) Hirsimäli, M.; Pitkänen, T.; Valden, M.; Lindroos, M.; Barnes, C. J. *Surf. Sci.* **2000**, *454*−*456*, 6.
(22) Tian, Y.; Quinn, J.; Lin, K.-W.; Jona, F. *Phys. Rev. B* **2000**, *61*, 4904.
(23) Ismail; Chandravakar, S.; Zehner, D. M. *Surf. Sci. Lett.* **2002**, *504*, L201.
(24) Hu, P.; Barnes, C. J.; King, D. A. *Phys. Rev. B* **1992**, *45*, 13595.
(25) Held, G.; Uremovic, S.; Stellwag, C.; Menzel, D. *Rev. Sci. Instrum.* **1996**, *67*, 378.
(26) CLEED manual; Held, G.; Braun, W., available from the authors.
(27) Pendry, J. B. *Low Energy Electron Diffraction*; Academic Press: London, UK, 1974.
(28) Van Hove, M. A.; Tong, S. Y. *Surface Crystallography by LEED*; Springer Series in Solid-State Sciences; Springer: Berlin, Germany, 1979.
(29) Tanuma, S.; Powell, C. J.; Penn, D. R. *Surf. Interface Anal.* **1991**, *17*, 911.
(30) Ashcroft, N. W.; Mermin, N. D. *Solid State Physics*; Holt-Saunders International Edition: Philadelphia, Pennsylvania, 1st ed., 1981.
(31) Phase shift program package. Barbieri, A.; Van Hove, M. A., available from http://electron.lbl.gov/software/software.html.
(32) Press, W. H.; Flannery, B. P.; Teukolsky, S. A.; Vetterling, W. T. *Numerical Recipes in C*; Cambridge University Press: Cambridge, UK, 1988.
(33) Nedler, J. A.; Mead, R. *Comput. J.* **1965**, *7*, 308.
(34) Pendry, J. B. *J. Phys.* **1980**, *C13*, 937.
(35) Held, G.; Bessent, M. P.; Titmuss, S.; King, D. A. *J. Chem. Phys.* **1996**, *105*, 11305.
(36) Van Hove, M. A.; Weinberg, W. H.; Chan, C.-M. *Low-Energy Electron Diffraction*; Springer Series in Surface Sciences; Springer: Berlin, Germany, 1986.
(37) Andersen, J. N.; Nielsen, H. B.; Petersen, L.; Adams, D. L. *J. Phys. C* **1984**, *17*, 173.
(38) CASTEP 3.9 academic version, licensed under the UKCP-MSI agreement, 1999−2001.
(39) Payne, M.; Teter, M.; Allan, D.; Arias, T.; Joannopoulos, J. *Rev. Mod. Phys.* **1992**, *64*, 1045.
(40) Monkhorst, H. J.; Pack, J. D. *Phys. Rev. B* **1976**, *13*, 5188.
(41) Perdew, J. P.; Chevary, J. A.; Vosko, S. H.; Jackson, K. A.; Pederson, M. R.; Singh, D. J.; Fiolhais, C. *Phys. Rev. B* **1992**, *46*, 6671.
(42) Vanderbilt, D. *Phys. Rev. B* **1990**, *41*, 7892.
(43) Held, G.; Jones, L. B.; Seddon, E. A.; King, D. A. *J. Phys. Chem. B* **2005**, *109*, 6159.
(44) Heilmann, P.; Heinz, K.; Müller, K. *Surf. Sci.* **1978**, *83*, 487−497.
(45) Linderoth, T. R.; Morthensen, J. J.; Jacobsen, K. W.; Lægsgaard, E.; Stensgaard, I.; Besenbacher, F. *Phys. Rev. Lett.* **1996**, *77*, 87.
(46) Feibelman, P. J. *Surf. Sci.* **1996**, *360*, 297.
(47) Menzel, D. *Surf. Rev. Lett.* **1997**, *6*, 1283.